The fasciola cinereum of the hippocampus is important in the acquisition, but not the retrieval, of visual contextual memory

Seong-Beom Park[1], Seung-Woo Yoo[1†], Hyun-Suk Jung[1], Heung-Yeol Lim[1], Eunsoo Lee[2], Woong Sun[2], and Inah Lee[1*]

[1]Department of Brain and Cognitive Sciences
Seoul National University
Gwanak-ro 1, Shillim-dong, Gwanak-gu
Seoul, Korea 08826

[2]Department of Anatomy
College of Medicine
Korea University
Anam-dong 5, Seongbuk-gu
Seoul, Korea 02841

[†]*Current address*
FAU Brain Institute
Florida Atlantic University
5353 Parkside Drive, Jupiter
FL 33458, USA

[*]**Corresponding author**
Inah Lee, Ph.D.
E-mail: inahlee@snu.ac.kr
Phone: +82-2-880-8013

Keywords
Hippocampus, Spatial Memory, Navigation, Episodic Memory, Scene Memory

Acknowledgments
This study was supported by grants from the BK21+ program (5286-2014100), Basic Research Laboratory Program (2018R1A4A1025616), and the Brain Research Program (2016R1A2B4008692, 2017M3C7A1029661).

Abstract

The fasciola cinereum (FC) is a small subregion of the hippocampus that has been relatively unattended and less known compared with other subregions with respect to anatomical characteristics and functional significance. The lack of a detailed anatomical characterization of the FC has created ambiguity in the literature regarding the definition of FC borders with the CA1 subregion and attribution of cognitive functions to specific subregions of the hippocampus. Here, we show that the anatomical borders of the FC can be clearly defined histologically, and the region itself is characterized by unique anatomical connections and physiological properties. The major output of the FC is to the dentate gyrus (DG) and the FC itself. Firing properties of cells recorded from the FC were different from those in the CA1, and no sign of neurogenesis was detected in the FC. Selective ablation of neurons in the FC, successfully accomplished using colchicine, significantly impaired acquisition of novel visual-contextual memory in rats, without affecting retrieval of familiar visual-contextual memories. Our findings suggest that, given its connections to the DG, the FC may play critical roles in learning novel contextual behavior.

The hippocampus is important for spatial navigation[1] and episodic memory[2], and specific computational roles have been assigned to its major subregions[3-9]. The fasciola cinereum (FC), a relatively small subregion of the hippocampus (Fig. 1a), has been largely ignored in the literature in terms of its anatomical and physiological characteristics as well as cognitive functions compared with other frequently studied subregions. Some early anatomical studies reported that cells in the FC resembled granule cells in the DG[10] and received inputs from the lateral entorhinal cortex (LEC) in rats[11], and that some similarities in genetic profiles existed between the FC and CA2 in mice (Table 1). However, the lack of detailed anatomical characterizations has created seeming inconsistencies in the literature regarding the distal borders of the CA1—the subregion immediately adjacent to the FC[12-15]. Furthermore, whether the FC is an extension of the DG[11] or CA2[16], or is an independent subregion in itself, is a matter of controversy.

Consistent with literature reports, the FC subregion is clearly defined by its sharp borders in Timm's-stained sections[17]. The abrupt changes in cell density in thionin-stained sections also support such distinct boundaries (Fig. 1b). To determine whether the FC is characterized by uniquely expressed markers compared with other hippocampal subregions[18], we immunostained sections for RGS14 (regulator of G-protein signaling 14), a genetic marker for both the FC and CA2[19]. We also immunostained for WFS1 (Wolfram syndrome 1), a marker for the CA1[20]. These analyses revealed distinct boundaries between the FC and CA1, matching the borders identified by Nissl and Timm's staining (Fig. 1c). A three-dimensional reconstruction showed that the FC constituted a longitudinal strip along the entire dorsal hippocampus (Fig. 1d).

There have been some disagreements in the literature with respect to the boundaries of the FC. Specifically, some studies have viewed the FC as an extension of the CA2 region, presumably based on similarities in their gene expression profile[16] (Table 1), whereas others have described the FC as a part of the DG[11]. To better delineate the FC boundaries in terms of its connectivity with other areas, we injected a retrograde tracer (Retrobeads; Lumafluor) into the FC (Fig. 2a). Retrobeads were found mostly in parahippocampal regions, including layer II of the LEC and layer II/III of the perirhinal cortex (PER) (Fig. 2a and 2b). In the posterior part of the LEC, Retrobeads were also found along the border between the LEC and postrhinal cortex (Fig. 2a and Supplementary Fig. 1a). Retrobeads were sparsely found in the

lateral part of the supramammillary area (Supplementary Fig. 1b). Interestingly, Retrobeads were also found in the FC itself along the longitudinal axis (Fig. 1b), suggesting intrinsic connectivity within the FC.

To identify efferent targets of the FC, we injected the FC with adeno-associated virus expressing the fluorescent marker mCherry (AAV-mCherry) or enhanced green fluorescent protein (AAV-EGFP). Axons of the FC were found in the molecular layer of the crest of the septal DG (Fig. 2c) and within the FC itself (Fig. 2d). The FC also projected to the septohippocampal nucleus, septofimbrial nucleus, indusium griseum and the septal tip of the Cornu Ammonis, but did not project to the CA1 (Supplementary Fig. 1c–1e). Retrobeads injected into the crest of the DG were found in the FC along the longitudinal axis, confirming the results of our anterograde tracing study (Fig. 2e). The boundaries of the FC and CA1 were also confirmed by injecting Retrobeads into the subiculum, a major output area of the CA1 (Supplementary Fig. 1f). Our findings suggest that the FC is unique among hippocampal subregions for its major projections to the DG only, and not to other traditional subregions, such as the CA3 and CA1.

Some prior studies considered the FC to be part of the DG[11]. However, these two subregions have different efferent targets, as noted above (Fig. 2c), and also show different gene expression patterns (Table 1). In addition, there are some critical differences with respect to neurogenesis in these two subregions[21]. Specifically, following intraperitoneal injection of BrdU for 7 days to label adult-born cells in the DG, neurons labeled with BrdU ($BrdU^+/NeuN^+$ cells) were found in the DG, but not in the FC (Fig. 3a). Although $BrdU^+$ cells were observed sparsely in the FC, these cells were glial cells rather than neurons, as evidenced by their expression of the oligodendroblast marker $NG2^+$ and absence of NeuN expression (Fig. 3b and 3c). These results suggest that the FC is an anatomically distinct subregion of the hippocampus that is separate from the DG.

The abovementioned anatomical results, particularly the anatomical border separating the FC from the CA1, were also physiologically validated. To achieve this, we compared the neurophysiological characteristics of the distalmost part of the CA1 (dmCA1), a region considered to be the FC in some studies[12,13], with the more laterally positioned distal CA1 (dCA1) and the FC (see Figure 1 and prior studies[14,15,17]). To lower tetrodes into the FC

while avoiding the superior sagittal sinus, we angled the tip of a hyperdrive 20° medially and implanted it 10° laterally from the vertical axis (Fig. 4a). Histological results showed that the tetrodes covered the FC, dmCA1, and dCA1 (Fig. 4a). Putative complex-spiking neurons were recorded in the FC (n = 48), dmCA1 (n = 182), and dCA1 (n = 104) of rats while the rats randomly foraged in a square arena (Fig. 4b and 4c). During foraging, cells in the FC fired in a place-specific manner that was seemingly indistinguishable by visual comparison of rate maps of place cells recorded in the FC and the CA1 (Fig. 4c). However, there were some notable differences in neuronal firing properties among subregions. Spikes recorded from cells in the FC exhibited narrower spikes compared with those in the dmCA1 and dCA1 (Fig. 4d). Moreover, basic firing patterns, such as average firing rate, peak firing rate and in-field firing rate, of neurons in the FC were significantly different from those of neurons in the dmCA1 and dCA1 ($p < 0.05$ for all; Fig. 4d). However, we found no significant difference in these measures between the dmCA1 and dCA1, suggesting that the FC and dmCA1 are physiologically differentiated from each other, whereas the dmCA1 and dCA1 are not (Supplementary Table 2). These results suggest that the sharp boundaries between the FC and CA1 are identifiable both anatomically and physiologically.

We next sought to determine the functional significance of the FC. Given the prominent efferent connections from the FC to the DG, we tested the roles of the FC in a DG-dependent task in rats[22]. Because granule cells are present in both the DG and FC[10], we were able to selectively lesion the FC by injecting it with colchicine (0.05 μL/site), a neurotoxin known to cause selective degenerative effects on the DG[23,24], while leaving the adjacent CA1 area relatively unaffected (Fig. 5a). Rats were tested in a modified version of the task previously used to test DG functions[22]. In this task, rats were administered a forced-choice paradigm in which they were required to make a left or right turn (an acrylic blocker prevented them from choosing the other arm) in association with a visual scene presented in the LCD monitors (Fig. 5b and 5c). During test trials in the final block, the blocker was removed and rats were allowed to freely choose the left or right arm (Fig. 5c). Once rats were trained to criterion, sham or colchicine lesions (n = 8 for each group) were made in the FC (Fig. 5c). After 2 weeks of recovery, rats were tested every other day using familiar and novel scenes. A histological verification of lesions resulted in exclusion of some rats from the lesion group either because no lesion was produced or extensive lesions were found (Supplementary

Table. 4), leaving a total of five rats in the lesion group.

The performance of rats in the lesion group was comparable to that of rats in the control group when familiar visual scenes were presented (OLD1), but learning behavior associated with novel visual scenes was significantly impaired in lesioned rats (control vs. lesion: OLD1, $p > 0.5$; NEW, $p < 0.01$; OLD1-NEW, $p = 0.01$; Fig. 5d and Supplementary Table. 3). To test the possibility that the performance deficits in the lesion group were attributable to factors unrelated to learning, we tested memory retrieval for familiar scenes again on day 18 (2 days after the acquisition of the new scenes). However, both control and lesion groups showed similar levels of performance ($p > 0.5$, Fig. 5e), and there was no significant difference between groups with respect to choice latency during acquisition ($p = 0.13$, Fig. 5f).

Interestingly, a comparison of the latency of rats on the stem (where the choice was made) between later trials of the first sample block (black screen only) and the following trial (peacock scene in Fig. 5g and 5h) showed that controls exhibited an abrupt increase in latency on the stem when the visual scene was first presented in trial 11, presumably because they noticed the changes in their visual background. However, no such novelty-detection–related behavior was observed in FC-lesioned rats [trial 10 vs. trial 11: control, $p < 0.01$; lesion, $p > 0.5$; control vs. lesion (t11/t10), $p = 0.001$] (Fig. 5g–5i). No increase in latency immediately after the introduction of the novel scene was observed in trial 12 (t12, control vs. lesion: $p > 0.1$; Fig. 5i), suggesting that the role of the FC in learning new visual contextual behavior is critical during the initial phase of the acquisition.

Discussion

In the current study, we demonstrated that the FC of the hippocampus is an independent subregion with distinct anatomical and physiological differences from other subregions of the hippocampus. The boundaries of the FC were clearly defined using various anatomical assays, and the FC itself showed unique afferent and efferent connections with both hippocampal and parahippocampal subregions. We verified these anatomical boundaries by

examining physiological characteristics of cells in the FC. The FC plays important roles in encoding a new visual context by detecting a contextual change, as evidenced by the fact that rats without a functional FC showed impaired acquisition of contextual behavior using novel visual background scenes.

The anatomical boundaries of the FC reported in the current study generally match those reported in prior studies[14,17], although some previous studies reported more extended lateral boundaries of the FC[12,13]. The more laterally extended boundaries of the FC toward the CA1 would inevitably shift the boundaries of the distal CA1 more toward the proximal CA1, possibly causing an erroneous characterization of the functions of the distal CA1. This is because it has been demonstrated that proximal and distal divisions of the CA1 receive differential inputs from the MEC and LEC, respectively; moreover, several prior studies characterized differences in the firing properties of cells along the proximodistal axis in the CA1[13,25,26]. Therefore, it is very important to clearly define the boundaries between the FC and CA1 so as to avoid mischaracterization of the physiological and functional properties of the most distal CA1 region of the hippocampus.

Our findings suggest that the most salient inputs of the FC come largely from the PER and LEC, whereas the FC sends its major outputs to the crest of the DG. Interestingly, these afferent and efferent regions of the FC have been relatively poorly characterized (compared with other regions, such as the MEC and the CA1) with respect to their roles in contextual and spatial information processing in the hippocampus[27-30]. Recent studies have raised the possibility that parahippocampal regions may not be as sharply segregated functionally as had been proposed[31-34], and suggested that theoretical modifications may be necessary[35-37]. In the current study, rats without a functional FC navigated mazes normally, but were impaired with respect to early detection of novel visual context compared with controls. Collectively, these results suggest that the FC may work together with a specific set of parahippocampal regions as well as the DG to detect visual contextual novelty in the animal's surroundings, possibly by facilitating pattern separation in the DG. The FC may do this by helping the DG to quickly set up sparse and orthogonal representations[3,4,38]. The intrinsic connections within the FC reported in the current study may also play important roles during contextual-novelty detection and encoding of a new visual context.

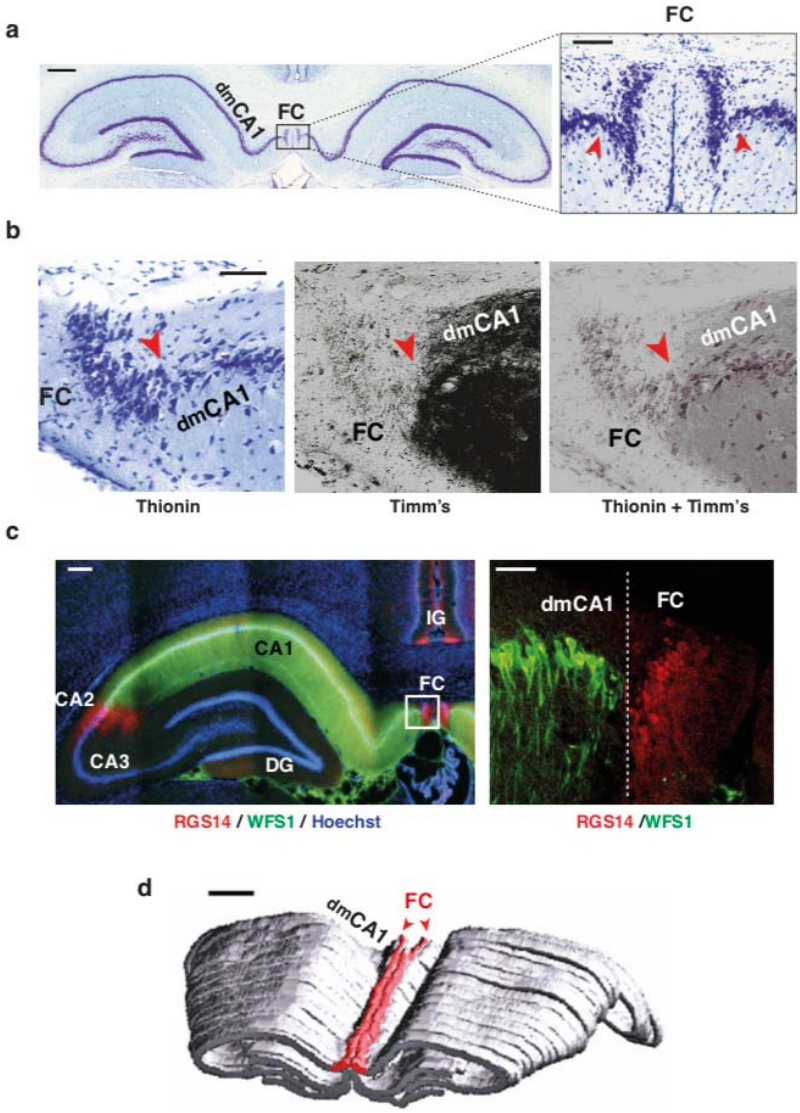

Figure 1. Anatomical characteristics of the FC. a. The FC in the hippocampus. The FC is located between the midline of the brain and the distalmost region of the CA1 (dmCA1) in Nissl-stained tissue. Scale bar: 500 μm. *Inset*: Magnified view of the FC and its boundaries (red arrowheads). Scale bar: 100 μm. **b**. The border between the FC and dmCA1. The lateral border of the FC is clearly visible (red arrowhead) in thionin-stained (*left*), Timm's-stained (*middle*), and merged (*right*) sections. Scale bar: 50 μm. **c**. Differential gene expression across hippocampal subfields. The expression of RGS14 (red) was only detected in the FC and CA2 in the hippocampus, whereas WFS1 expression (green) was only found in the CA1. Scale bar: 250 μm. *Inset*: Magnified view of the white-boxed area. Scale bar: 50 μm. **d**. Three-dimensional view of the FC in the hippocampus. The FC region (red) runs along the longitudinal axis of the dorsal hippocampus, adjoining the dmCA1 (arrowheads). Scale bar: 1 mm.

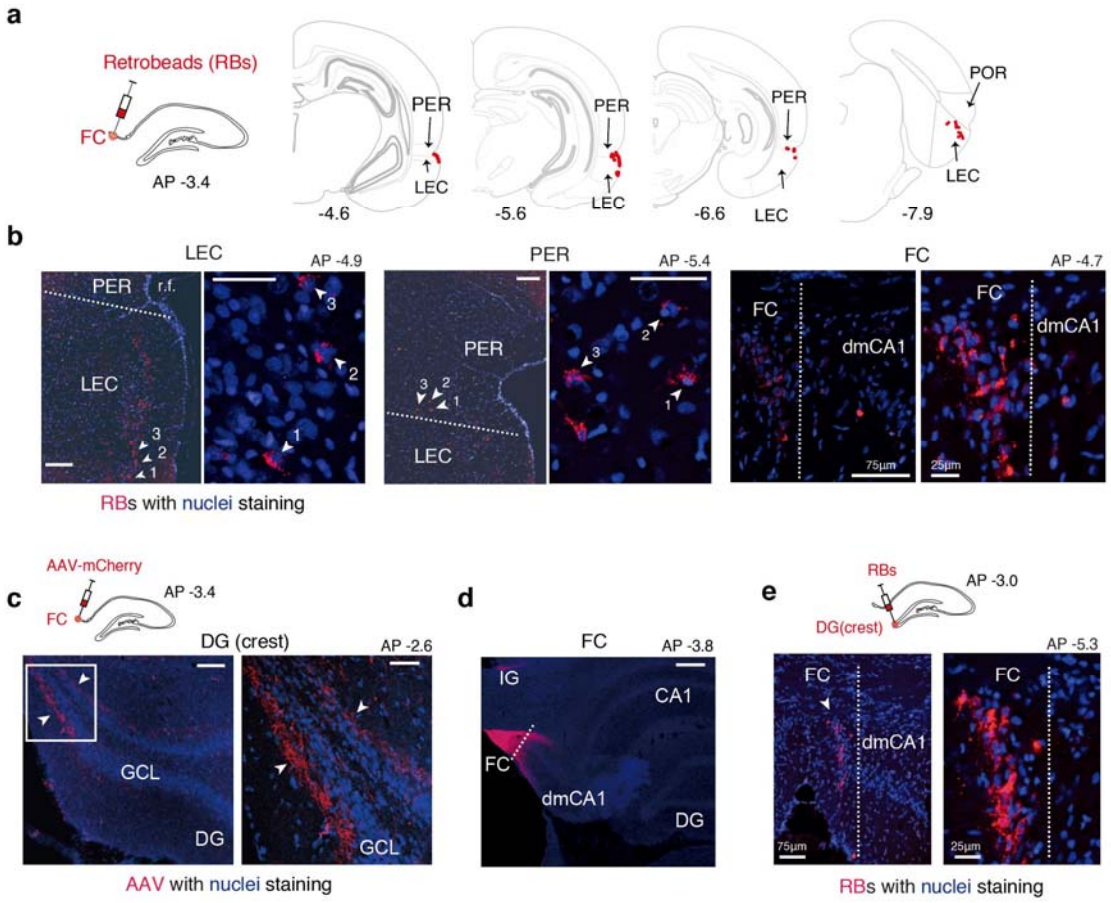

Figure 2. Anatomical connections of the FC. a. Afferent regions of the FC. Retrograde tracing of afferent connectivity was conducted by injecting Retrobeads (RBs) in the FC. Locations with RB-containing cells (red dots) were marked on the atlas (modified from the study of Paxinos and Watson; parahippocampal boundaries are after the Burwell study[15,39]). Numbers indicate the relative positions of sections from bregma. RBs were detected mostly in layer II of the LEC and the layer II-III in the PER (A35). Posteriorly, RBs were found in deeper layers of the LEC adjoining the borders with the postrhinal cortex (POR). **b**. Retrograde labeling of cells projecting to the FC. Nuclei and RBs are shown in blue (Hoechst staining) and red, respectively. Cells projecting to the FC were found in the LEC (*left*) and PER (*middle*). Intrinsic connections within the FC are also shown (*right*). dmCA1, distalmost CA1. **c**. FC projections to the DG. Axons of FC cells containing AAV-mCherry (red; injected into the FC) were detected in the molecular layer (ML) of the crest of the septal DG. White arrowheads indicate axons immediately adjacent to the granule cell layer (blue; stained with DAPI). GCL, granule cell layer. **d.** Anterograde transport of AAV-mCherry within the FC itself via intrinsic connections was also detected. IG, indusium griseum. **e.** RBs injected into the crest of the DG were transported retrogradely to the FC.

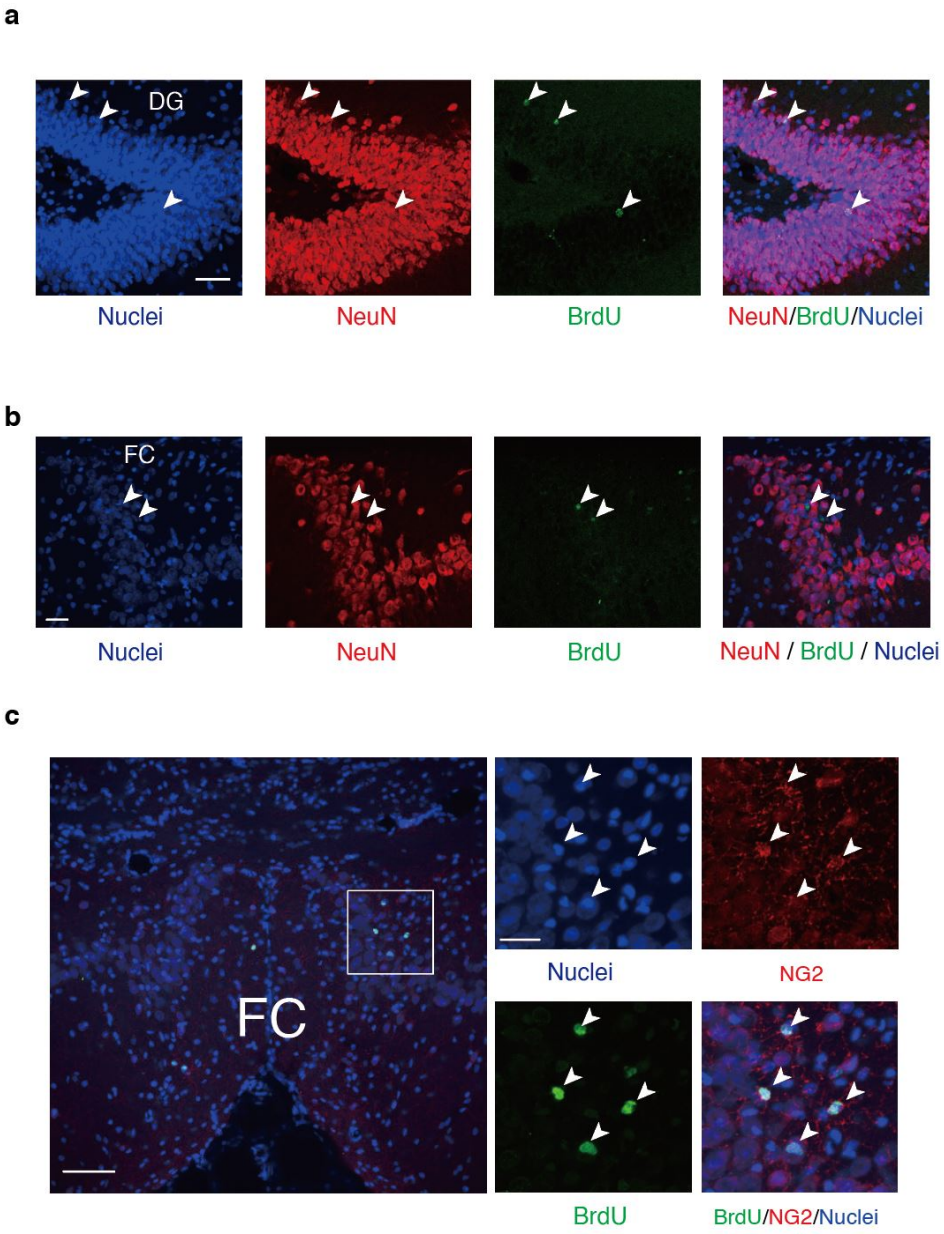

Figure 3. No evidence of neurogenesis in the FC. a. Some granule cells ($NeuN^+$, red; left) in the DG are newborn cells ($BrdU^+$, green; middle), marked by arrowheads. A merged image of the two photomicrographs (NeuN+BrdU) with the nuclei-stained section (Hoechst staining, blue; right) showed the presence of adult-born granule cells in the DG (white; arrowheads). Scale bar: 50 μm. **b.** In the FC, the locations of $BrdU^+$ cells (arrowheads) did not overlap with the locations of $NeuN^+$ cells. Scale bar: 30 μm. **c.** BrdU-labeled cells in the FC were co-localized with NG2-labeled glial cells (oligodendroblasts; arrowhead). Scale bars: 75 μm(*left*) and 25 μm (*right*).

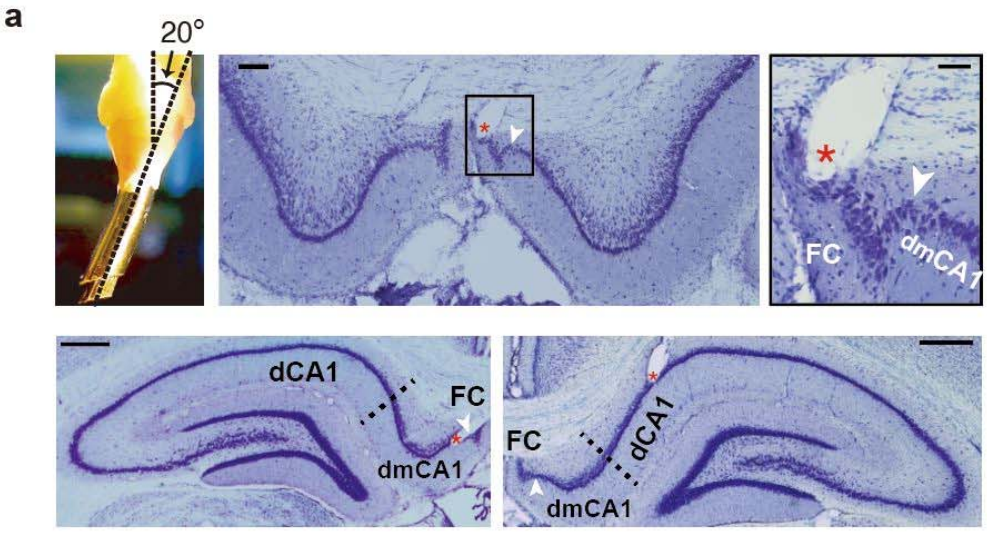

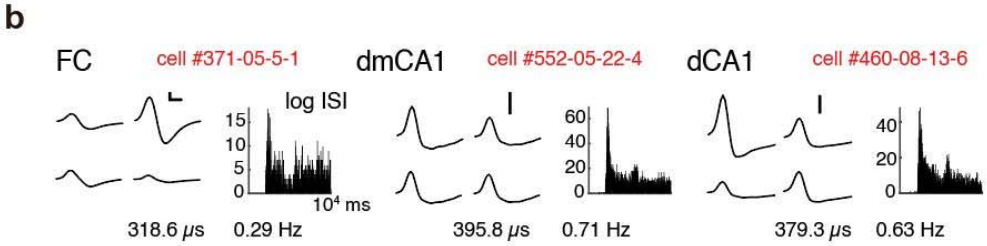

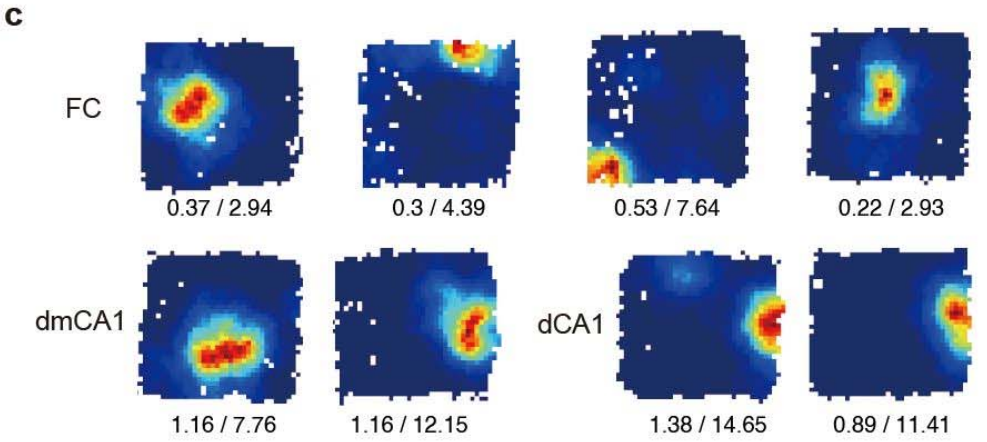

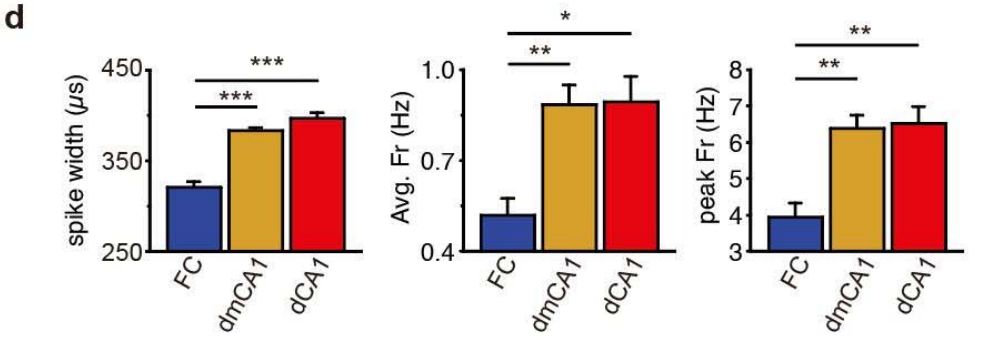

Figure 4. Physiological boundaries between the FC and CA1. a. Recording electrode bundle and tetrode locations. *Upper left:* An angled bundle (20° medially) carrying 24 tetrodes to the FC and its neighboring hippocampal subregions was installed in the hyperdrive. *Upper center:* Representative example of the electrode track, showing the tetrode tip in the cell layer of the FC. *Upper right:* Magnified view more clearly showing the tip location (*). Tetrode tracks that recorded the distalmost CA1 (dmCA1; *lower left*) and distal CA1 (dCA1; *lower right*) regions are also shown. Scale bars: 100 μm (*upper center*), 50 μm (*upper right*) and 500 μm (lower panels). **b.** Single unit waveforms. Representative waveforms (*left*) and inter-spike interval (ISI) histograms (log scale) of single units recorded from the FC, dmCA1, and dCA1 are shown. Vertical scale bar: 100 μV; horizontal scale bar: 200 μs. Numbers below the plots indicate (left to right) spike width and firing rate in a recording session during rest. **c.** Representative place fields of principal cells in the FC, dmCA1 and dCA1, recorded during foraging in a square arena. The numbers below are mean firing rates and peak firing rates of place cells. **d.** Comparison among the FC dmCA1 and dCA1. Place cells in the FC showed different firing patterns compared with those in the dmCA1 and dCA1 in terms of spike width, mean firing rate, and peak firing rate (*$p<0.05$, **$p < 0.01$, ***$p<0.001$).

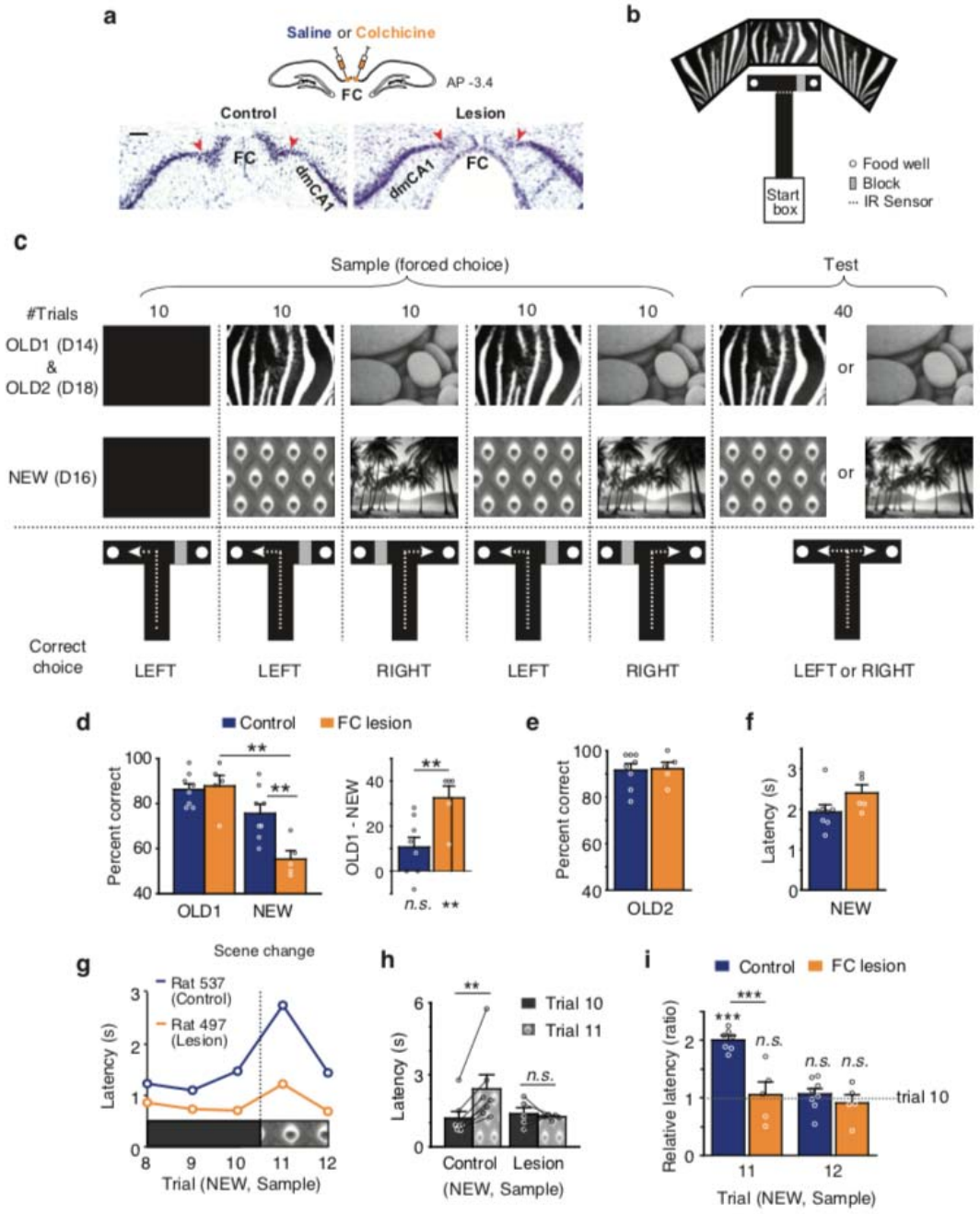

Figure 5. FC lesions impair acquisition, but not retrieval, of hippocampal memory. a. Selective lesioning of the FC with colchicine. Selective lesions of the FC in the lesion group, compared with the intact FC in the control group (Nissl staining). Arrowheads mark the boundaries between the FC and dmCA1. Scale bar: 100 μm. **b.** Behavioral apparatus. The white dotted line indicates the point where the infrared beam sensors were installed. The gray rectangle represents the acrylic block used to restrict access to the arm. **c.** Experimental schedule and behavioral paradigm. Rats were trained with familiar scenes before surgery. After a recovery period (14 days), rats were tested with the same scenes for one day (OLD1), then experienced two more sessions with new scenes (NEW), and re-experienced old scenes (OLD2) with a 1-day rest between sessions. In a single session, a rat experienced a total of 90 trials (50 sample trials and 40 test trials). Sample trials consisted of 5 blocks (10 trials per block). **d.** Deficits in the acquisition, but not retrieval, of scene memory in the FC lesion group. Data represent means ± S.E.M. (**p < 0.01). *Right:* Same data replotted using the difference in performance (OLD1 – NEW). **e–f.** No significant difference in performance in the OLD2 session (e), and no significant difference in latency during testing in the NEW session (f) between control and lesion groups. **g–i.** Differential responses to initial introduction of the novel scene (peacock feather pattern) between control and lesion groups. Representative example from one rat (g) and the average latency (raw and ratio) between trial 10 and 11 for all rats are shown (h, i). Data represent means ± S.E.M. (***p < 0.001).

Table 1. Genes known to be expressed in FC and CA2 subregions based on the literature. Genes expressed throughout hippocampal subregions, such as CamKII (Ca^{2+}/calmodulin-dependent protein kinase II) and GAD67 (glutamate decarboxylase 67) were excluded.

Gene	Full name	Reference	Note
Genes expressed in the both FC and CA2			
Pcp4	Purkinje cell protein 4	Lein et al.[18]	Also observed in the DG
Amigo2	Adhesion molecule with Ig-like domain 2	Laeremans et al.[16]	Also observed in the CA3a
bFGF	Fibroblast growth factor 2	Lippoldt et al.[40]	
NT-3	Neurotrophin-3	Vigers et al.[41]	
RGS14	Regulator of G-protein signaling 14	Lee et al.[19]	
OX_1R	Orexin receptor 1	Marcus et al.[42]	Also observed in the crest of the septal DG
Cx30.2	Connexin 30.2	Kreuzberg et al.[43]	
Nestin	Nestin	Hendrikson et al.[44]	
Ncald	Neurocalcin-δ	Girard et al.[45]	
Gene expressed only in the FC, and not in other hippocampal subregions			
RgmA	Repulsive guidance molecule A	Schmidtmer and Engelkamp[46]	RgmA is restricted to the FC in adult mice, but not in young animals[47,48]
Genes expressed in the CA2, but not in the FC			
Avpr1b	Vasopressin 1b receptor	Pagani et al.[49]	
S100b	S100 protein, beta polypeptide, neural	Girard et al.[45]	

References

1 Morris, R. G., Garrud, P., Rawlins, J. N. & O'Keefe, J. Place navigation impaired in rats with hippocampal lesions. *Nature* **297**, 681-683 (1982).

2 Scoville, W., B, & Milner, B. Loss of recent memory after bilateral hippocampal lesions. *J.Neurol.Neurosurg.Psychiatry* **20**, 11-21 (1957).

3 Marr, D. Simple memory: a theory for archicortex. *Philosophical transactions of the Royal Society of London. Series B, Biological sciences* **262**, 23-81, doi:10.1098/rstb.1971.0078 (1971).

4 O'Reilly, R. C. & McClelland, J. L. Hippocampal conjunctive encoding, storage, and recall: avoiding a trade-off. *Hippocampus* **4**, 661-682, doi:10.1002/hipo.450040605 (1994).

5 Treves, A. & Rolls, E. T. Computational analysis of the role of the hippocampus in memory. *Hippocampus* **4**, 374-391, doi:10.1002/hipo.450040319 (1994).

6 Lee, I., Yoganarasimha, D., Rao, G. & Knierim, J. J. Comparison of population coherence of place cells in hippocampal subfields CA1 and CA3. *Nature* **430**, 456-459 (2004).

7 Leutgeb, S., Leutgeb, J. K., Treves, A., Moser, M.-B. & Moser, E. I. Distinct Ensemble Codes in Hippocampal Areas CA3 and CA1. *Science* **305**, 1295-1298 (2004).

8 Vazdarjanova, A. & Guzowski, J. F. Differences in hippocampal neuronal population responses to modifications of an environmental context: evidence for distinct, yet complementary, functions of CA3 and CA1 ensembles. *The Journal of neuroscience : the official journal of the Society for Neuroscience* **24**, 6489-6496, doi:10.1523/JNEUROSCI.0350-04.2004 (2004).

9 Neunuebel, J. P. & Knierim, J. J. CA3 retrieves coherent representations from degraded input: direct evidence for CA3 pattern completion and dentate gyrus pattern separation. *Neuron* **81**, 416-427, doi:10.1016/j.neuron.2013.11.017 (2014).

10 Hjorth-Simonsen, A. & Laurberg, S. Commissural connections of the dentate area in the rat. *The Journal of comparative neurology* **174**, 591-606, doi:10.1002/cne.901740404 (1977).

11 Hjorth-Simonsen, A. Projection of the lateral part of the entorhinal area to the hippocampus and fascia dentata. *The Journal of comparative neurology* **146**, 219-232, doi:10.1002/cne.901460206 (1972).

12 Boccara, C. N. *et al.* A three-plane architectonic atlas of the rat hippocampal region. *Hippocampus* **25**, 838-857, doi:10.1002/hipo.22407 (2015).

13 Henriksen, E. J. *et al.* Spatial representation along the proximodistal axis of CA1. *Neuron* **68**, 127-137, doi:10.1016/j.neuron.2010.08.042 (2010).

14 Swanson, L. W. Brain maps 4.0-Structure of the rat brain: An open access atlas with global nervous system nomenclature ontology and flatmaps. *The Journal of comparative neurology* **526**, 935-943, doi:10.1002/cne.24381 (2018).

15 Paxinos, G. & Watson, C. *The rat brain in stereotaxic coordinates: compact sixth edition*. (New York, NY: Academic Press, 2009).

16 Laeremans, A. *et al.* AMIGO2 mRNA expression in hippocampal CA2 and CA3a. *Brain structure & function* **218**, 123-130, doi:10.1007/s00429-012-0387-4 (2013).

17 Haug, F. M. Light microscopical mapping of the hippocampal region, the pyriform cortex and the corticomedial amygdaloid nuclei of the rat with Timm's sulphide silver method. I. Area dentata, hippocampus and subiculum. *Z Anat Entwicklungsgesch* **145**, 1-27 (1974).

18 Lein, E. S., Callaway, E. M., Albright, T. D. & Gage, F. H. Redefining the boundaries of the hippocampal CA2 subfield in the mouse using gene expression and 3-dimensional reconstruction. *The Journal of comparative neurology* **485**, 1-10, doi:10.1002/cne.20426 (2005).

19 Lee, S. E. *et al.* RGS14 is a natural suppressor of both synaptic plasticity in CA2 neurons and hippocampal-based learning and memory. *Proceedings of the National Academy of Sciences of the United States of America* **107**, 16994-16998, doi:10.1073/pnas.1005362107 (2010).

20 Takeda, K. *et al.* WFS1 (Wolfram syndrome 1) gene product: predominant subcellular localization to endoplasmic reticulum in cultured cells and neuronal expression in rat brain. *Hum Mol Genet* **10**, 477-484, doi:10.1093/hmg/10.5.477 (2001).

21 Altman, J. & Chorover, S. L. Autoradiographic Investigation of the Distribution and Utilization of Intraventricularly Injected Adenine-3h, Uracil-3h and Thymidine-3h in

the Brains of Cats. *J Physiol* **169**, 770-779, doi:10.1113/jphysiol.1963.sp007295 (1963).

22 Ahn, J. R. & Lee, I. Intact CA3 in the hippocampus is only sufficient for contextual behavior based on well-learned and unaltered visual background. *Hippocampus* **24**, 1081-1093, doi:10.1002/hipo.22292 (2014).

23 Lee, I. & Kesner, R. P. Differential contributions of dorsal hippocampal subregions to memory acquisition and retrieval in contextual fear-conditioning. *Hippocampus* **14**, 301-310 (2004).

24 Walsh, T. J., Schulz, D. W., Tilson, H. A. & Schmechel, D. E. Colchicine-induced granule cell loss in rat hippocampus: selective behavioral and histological alterations. *Brain Res* **398**, 23-36 (1986).

25 Steward, O. Topographic organization of the projections from the entorhinal area to the hippocampal formation of the rat. *The Journal of comparative neurology* **167**, 285-314, doi:10.1002/cne.901670303 (1976).

26 Sun, Y., Nitz, D. A., Holmes, T. C. & Xu, X. Opposing and Complementary Topographic Connectivity Gradients Revealed by Quantitative Analysis of Canonical and Noncanonical Hippocampal CA1 Inputs. *eNeuro* **5**, doi:10.1523/ENEURO.0322-17.2018 (2018).

27 Fyhn, M., Molden, S., Witter, M. P., Moser, E. I. & Moser, M. B. Spatial representation in the entorhinal cortex. *Science* **305**, 1258-1264, doi:10.1126/science.1099901 (2004).

28 Hafting, T., Fyhn, M., Molden, S., Moser, M. B. & Moser, E. I. Microstructure of a spatial map in the entorhinal cortex. *Nature* **436**, 801-806, doi:10.1038/nature03721 (2005).

29 Lee, H. W., Lee, S. M. & Lee, I. Neural Firing Patterns Are More Schematic and Less Sensitive to Changes in Background Visual Scenes in the Subiculum than in the Hippocampus. *The Journal of neuroscience : the official journal of the Society for Neuroscience* **38**, 7392-7408, doi:10.1523/JNEUROSCI.0156-18.2018 (2018).

30 O'Keefe, J. & Dostrovsky, J. The hippocampus as a spatial map: Preliminary evidence from unit activity in the freely-moving rat. *Brain Res* **34**, 171-175 (1971).

31 Eichenbaum, H., Yonelinas, A. P. & Ranganath, C. The medial temporal lobe and

recognition memory. *Annual review of neuroscience* **30**, 123-152, doi:10.1146/annurev.neuro.30.051606.094328 (2007).

32 Kerr, K. M., Agster, K. L., Furtak, S. C. & Burwell, R. D. Functional neuroanatomy of the parahippocampal region: the lateral and medial entorhinal areas. *Hippocampus* **17**, 697-708, doi:10.1002/hipo.20315 [doi] (2007).

33 Tomas Pereira, I., Agster, K. L. & Burwell, R. D. Subcortical connections of the perirhinal, postrhinal, and entorhinal cortices of the rat. I. afferents. *Hippocampus* **26**, 1189-1212, doi:10.1002/hipo.22603 (2016).

34 Hargreaves, E. L., Rao, G., Lee, I. & Knierim, J. J. Major dissociation between medial and lateral entorhinal input to dorsal hippocampus. *Science* **308**, 1792-1794, doi:10.1126/science.1110449 (2005).

35 Baldassano, C. *Visual Scene Perception in the Human Brain: Connections to Memory, Categorization, and Social Cognition*, Stanford University, (2015).

36 Park, E. H., Ahn, J. R. & Lee, I. Interactions between stimulus and response types are more strongly represented in the entorhinal cortex than in its upstream regions in rats. *Elife* **6**, doi:10.7554/eLife.32657 (2017).

37 Yoo, S. W. & Lee, I. Functional double dissociation within the entorhinal cortex for visual scene-dependent choice behavior. *Elife* **6**, doi:10.7554/eLife.21543 (2017).

38 GoodSmith, D. *et al.* Spatial Representations of Granule Cells and Mossy Cells of the Dentate Gyrus. *Neuron* **93**, 677-690 e675, doi:10.1016/j.neuron.2016.12.026 (2017).

39 Burwell, R. D. Borders and cytoarchitecture of the perirhinal and postrhinal cortices in the rat. *Journal of Comparative Neurology* **437**, 17-41 (2001).

40 Lippoldt, A. *et al.* Photochemically induced focal cerebral ischemia in rat: time dependent and global increase in expression of basic fibroblast growth factor mRNA. *Brain Res* **625**, 45-56 (1993).

41 Vigers, A. J., Baquet, Z. C. & Jones, K. R. Expression of neurotrophin-3 in the mouse forebrain: insights from a targeted LacZ reporter. *The Journal of comparative neurology* **416**, 398-415 (2000).

42 Marcus, J. N. *et al.* Differential expression of orexin receptors 1 and 2 in the rat brain. *The Journal of comparative neurology* **435**, 6-25 (2001).

43 Kreuzberg, M. M. *et al.* Expression of connexin30.2 in interneurons of the central

nervous system in the mouse. *Molecular and cellular neurosciences* **37**, 119-134, doi:10.1016/j.mcn.2007.09.003 (2008).

44 Hendrickson, M. L., Rao, A. J., Demerdash, O. N. & Kalil, R. E. Expression of nestin by neural cells in the adult rat and human brain. *PloS one* **6**, e18535, doi:10.1371/journal.pone.0018535 (2011).

45 Girard, F., Venail, J., Schwaller, B. & Celio, M. R. The EF-hand Ca(2+)-binding protein super-family: a genome-wide analysis of gene expression patterns in the adult mouse brain. *Neuroscience* **294**, 116-155, doi:10.1016/j.neuroscience.2015.02.018 (2015).

46 Schmidtmer, J. & Engelkamp, D. Isolation and expression pattern of three mouse homologues of chick Rgm. *Gene Expression Patterns* **4**, 105-110, doi:10.1016/s1567-133x(03)00144-3 (2004).

47 Brinks, H. *et al.* The repulsive guidance molecule RGMa is involved in the formation of afferent connections in the dentate gyrus. *The Journal of neuroscience : the official journal of the Society for Neuroscience* **24**, 3862-3869, doi:10.1523/JNEUROSCI.5296-03.2004 (2004).

48 Li, N. *et al.* Effects of maternal lead exposure on RGMa and RGMb expression in the hippocampus and cerebral cortex of mouse pups. *Brain Res Bull* **127**, 38-46, doi:10.1016/j.brainresbull.2016.08.010 (2016).

49 Pagani, J. H. *et al.* Role of the vasopressin 1b receptor in rodent aggressive behavior and synaptic plasticity in hippocampal area CA2. *Mol.Psychiatry* **20**, 490-499, doi:10.1038/mp.2014.47 (2015).

Supplementary Methods

Subject

Long-Evans (LE; n = 33) and Sprague-Dawley (SD; n = 51) rats were used in the study. Rats were individually housed with a 12-12 h light-dark cycle. All behavioral experiments were conducted during the light cycle. All protocols complied with the Institutional Animal Care and Use Committee of the Seoul National University.

Anatomical tracing

SD rats (9–24 weeks old) were used in the retrograde-tracing study (n = 31) and anterograde-tracing study (n=7). Rats were initially anesthetized with sodium pentobarbital (Nembutal, 65 mg/kg), and anesthesia was maintained by 1-2% isoflurane (Piramal, Bethlehem, PA) in a stereotaxic frame for cannula implantation. Small burr holes were drilled and commercial guide cannulae (26 G, Plastics One, Roanoke, VA) were implanted targeting the fasciola cinereum (FC), distalmost CA1 or DG. One or two cannulae were inserted using the following coordinates: (1) FC: -3.4 mm from bregma, 1.1-1.2 mm from midline, and 3.7 or 4.0 mm deep from dura at 20° angle, (2) CA1: -3.4 mm from bregma, -1.2 mm from midline, 3.0 mm deep from dura, (3) DG: -3.0 mm from bregma, 2.4 mm from midline, 4.3 mm deep from dura at 20° angle. (4) SUB: -5.2 mm from bregma, ±1.2 mm from the midline, 3.4 mm deep from the skull and -5.8 mm from bregma, ±5.8 mm from the midline, 3.2 mm deep from the skull. Guide cannulae were used in our tracing experiments to prevent the upward spread of tracer. Cannulae were fixed to the skull with dental cement and skull screws. Then, retrobeads were injected through the injection cannula (33G, Plastics One), protruding less than 0.5 mm from the tip of the guide cannula. The injection cannula was connected with 10 μl Hamilton syringe via polyethylene tubing (PE20, Becton Dickinson), and the injection was controlled by a micropump (KDS-101, KD Scientific). For retrograde tracing, retrobeads (30 nL of red or green retrobeads, Lumafluor) were injected at each injection site at 10 μL/h rate. The rat was sacrificed 3-10 days after the injection of retrobeads. For anterograde tracing, AAV–CMV-mCherry or eGFP[1] (Addgene plasmid # 49055; 0.03 or 0.05 μL; KIST, Seoul, Korea) was injected into the FC, and the rat was sacrificed three weeks after the injection. For

4 rats, AAV2/9.CaMKII.hChR2(E123A).mCherry.WPRE.hGH (0.02 μL; Catalog#: AV-9-35506, Addgene plasmid # 35506, Penn Vector Core, PA, USA)[2] was injected into the right FC via glass pipette controlled by a micropump (Legato 130, KD Scientific, MA, USA). The injection coordinates for the four rats were as follows: 3.5 mm posterior from bregma, 0.1 mm from the midline and 3.6 mm deep from dura without angle through the superior sagittal sinus.

Histological procedures

Rats were killed by the inhalation of CO2 overdose and were perfused transcardially with 0.1 M PBS, followed by 4% v/v formaldehyde. The brain was extracted and fixed in 30% sucrose-formalin at 4 °C. The brain was coated with gelatin with sucrose solution after it sank and was fixed again in sucrose formaldehyde solution for 1-2 days. The brain was sectioned at 35 μm using a freezing microtome (HM 430; Thermo Fisher Scientific). Every third sections were first stained for Nissl substances (Thionin staining). The adjacent sections were used for fluorescent photomicrography and staining for nuclei (Hoechst, Cat No. 33342, Thermo Fisher, 1:1000; DAPI, H-1200, Vectashield). Photomicrography was conducted using a fluorescent microscope (Eclipse 80i, Nikon) or confocal microscope (Leica TCS SP8, Leica). For delineating the boundaries, serial sections from one LE rat were stained with Thionin staining, Timm's staining, and myelin staining.

Neurogenesis

SD rats (12 weeks old; n = 10) were used. BrdU was dissolved in saline solution (30-50 mg/mL) and injected into a rat with 100 mg/kg concentration (intraperitoneal injection). The injection was performed at 1 pm – 4 pm for seven consecutive days. Five rats were transcardially perfused with 0.1M PBS solution followed by 4% formaldehyde solution at seven days after the last injection, and the others were sacrificed at 21 days after perfused with 4% paraformaldehyde. The brains were post-fixed in the same fixative for 24 h. Brains were then cryoprotected in 30% sucrose, sectioned serially (40um), and stored in 50% PBS solution with 50% glycerol at -20 ºC until use. For BrdU staining, 10mM sodium citrate buffer (pH 6.0) was pre-heated in the microwave for 7min, slides were immersed in the hot buffer. After 5 min, the buffer (with immersed slides) was reheated for 5 min using

microwave. The buffer with slides still immersed was allowed to cool for 30 min at room temperature. Immunohistochemical processing was then initiated beginning with a PBS wash of the slides and then blocking as described below. Primary antibodies against BrdU (1:300, Thermo Fisher Scientific, 1:500, abcam), NeuN (1:500, Millipore) and NG2 (1:500, Millipore) were applied for overnight at 4˚C with gentle shaking. After several washes with PBS, appropriate secondary antibodies were applied for 1 h by matching primary antibody host for fluorescence imaging. Subsequently, sections were washed and mounted. Images were acquired using a TCS SP8 confocal laser-scanning microscope (Leica, Germany).

Immunohistochemistry

To mark the boundaries between the FC and CA1, two SD rats (8 weeks old) were used in immunohistochemistry. Rats were anesthetized with an intraperitoneal injection of urethane and transcardially perfused with saline solution, followed by 4% paraformaldehyde (PFA) solution. The brain was extracted, and stored in 4% paraformaldehyde solution until it sank to the bottom of the tube, and transferred into 30% sucrose-formaldehyde solution or 30% sucrose solution. Coronal sections (40 μm) were frozen and cut on a sliding microtome. Then, sections were incubated with primary antibodies against RGS14 (1:300, NeuroMab) and WFS1(1:300, Proteintech) diluted in 3% BSA and 0.2% TritonX-100 in PBS for overnight at 4˚C. Sections were rinsed 3 times with PBS and incubated with the appropriate secondary antibodies (1:500, Invitrogen and Jackson immunoresearch laboratories) and Hoechst33342 (1:1000, Thermo Fisher Scientific) for 1 h at room temperature. The image was acquired using a TCS SP8 confocal laser-scanning microscope (Leica, Germany).

Place-cell recording

The experiment was carried out in a black square acrylic box (70 x 70 cm; 60 cm high). A white cue card (40 x 54 cm) was attached on the north wall. The box was surrounded with a black curtain and white noise was played through loudspeakers throughout the experiment for masking environmental noise. The floor of the square arena was covered with large brown paper, replaced between sessions to control local cues on the floor. A digital camera, commutator (PSR-36, Neuralynx), and a custom semi-automatic feeder were all installed in

the ceiling. The feeder scattered chocolate sprinkles when an experimenter pushed a switch from outside the testing room while monitoring the rat's movement.

Hyperdrive implantation surgery

Procedures for constructing and surgically implanting the hyperdrive can be found in detail in our previous articles[3] and will be only briefly described here. A hyperdrive with 24 tetrodes was custom-made and implanted in LE rats (11-41 weeks old; n = 12). Nichrome wires were used for tetrodes (17.8 μm in diameter, A-M systems). To avoid damage in the superior sagittal sinus, the tetrode-carrying bundle of the hyperdrive was angled at 20˚ to approach the FC obliquely. The hyperdrive itself was inserted into the brain also at 10˚ angle. The surgical coordinates were pre-calculated to target the FC on the right hemisphere with the tip of the tetrode bundle (9G or 12G stainless-steel tubing): 3.6 mm posterior to bregma and 2.2 mm lateral from midline. Stainless-steel wire coupled to the ground channel of the hyperdrive was connected to the skull screw over the cerebellum to be used as animal ground.

Electrophysiological recording procedures

After seven days of recovery from surgery, tetrodes were lowered daily to target areas (FC, CA1 or DG) for about three weeks. Spiking activities from single units and local field potentials (LFPs) were fed to the data-acquisition system (Digitalynx SX, Neuralynx) through an electrode interface board (EIB-36-24TT, Neuralynx), pre-amplifier (HS-36, Neuralynx), and tether (HS-36 Litz tether, Neuralynx). Signal was digitized at 32 kHz, filtered at 600-6,000 Hz, and amplified 1,000-10,000 times. When most of the tetrodes reached the target areas, a habituation session started in the foraging box with the tether connected to the hyperdrive at least for three days, followed by foraging sessions for 6–14 days. During the foraging sessions, rats freely moved around in the square box to consume chocolate sprinkles, and the hippocampal neural signals were recorded in sync with position and head-direction information for 15 min. Neural signals were recorded during sleep in a sound-attenuating booth outside the experimental room (sleep session) before and after each behavioral recording session. The rat was allowed to sleep in the booth for at least 30 min to provide enough neural data associated with the resting period.

Histological verification of electrode positions

After the last recording session, the rat was killed by CO_2 overdose and perfused transcardially with phosphate-buffered saline (PBS) followed by 4% v/v formalin solution. The head was fixed in formalin solution for one day before the brain was extracted. The extracted brain was fixed in 30% sucrose in 4% formaldehyde solution until it sank to the bottom of the tube at 4°C. Then, the brain was coated with gelatin and fixed in sucrose formaldehyde solution for 1-2 days. The brain was sectioned at 40 μm using a freezing microtome (HM 430, Thermo-Fisher Scientific), and every section was mounted on the glass slide and was thionin-stained. Photomicrographs were taken with a digital camera (DS-Fi1c, Nikon) attached to a microscope (Eclipse 80i, Nikon) and tetrode tracks were reconstructed three-dimensionally (Voxwin, UK) to match between the electrode track with the pre-configured bundle design. The recorded depth of tetrodes and physiological profiles were also considered during the reconstruction procedures.

Unit isolation

Single units were recorded simultaneously from the FC (n = 228), CA1 (n = 1195) and DG (n = 129), and unit isolation was manually performed using custom-written software (WinClust) using the peaks of waveforms as the major measure as described previously[3] while considering other parameters such as energy as well. Spikes collected during sleep sessions were also used during unit isolation for judging the stability of recording. Only the single units that meet the following criteria were included in analysis: (a) More than 50 spikes of a cluster should be identified in both the pre- and post-sleep sessions and the proportion of the number of spikes within a refractory period (1 ms) should be less than 1% of the total spikes, (b) Mean firing rate of a cluster should be less than 10 Hz to include only putative complex spiking neurons, (c) Only place cells (the number of spikes in the open field ≥ 50, spatial information ≥ 0.5 with p-value < 0.05; see 'Data Analysis' for details). Spikes recorded while the animal was relatively stationary (moment velocity < 5 cm/s) were filtered out and were not used in analysis[4]. For delineating the boundaries physiologically, we divided the CA1 to two subdivisions based on online atlas[5]: the distalmost part of the CA1 (dmCA1) that was regarded as the FC in some previous reports[4,5] and the distal CA1 (dCA1) that is located more medially compared to the dmCA1. Only the tetrodes posterior to AP -3.0 were used for

analysis.

Electrophysiological data analysis

Spike width was defined as the distance between the peak and trough of the averaged spike waveform. To construct a rate map, position data from the foraging session was binned into a matrix (bin size = 2.7 × 2.7 cm) and spike data were assigned to the matching bins. A rate map was calculated by diving the number of spikes by the duration of visit per bin (firing rate). The resulting rate map was smoothed by an adaptive binning method[6].

In a rate map of a unit, continuous bins showing over 20% of the peak firing rate were included to define the unit's place field. At least 20 continuous bins (88.2 cm^2) were required for the unit's firing field to be qualified as a place field. In-field firing rate was measured as the firing rate in the place field. The stability of a rate-map was measured as the correlation coefficient (R) between the rate maps constructed for the first half and the second half of a session (each half = 7.5 min)[4]. Spatial information of spiking activity was measured as follows[7].

$$\text{Spatial information} = \sum_i p_i \frac{\lambda_i}{\lambda} \log_2 \frac{\lambda_i}{\lambda} \text{ (bits/spike)},$$

where i denotes the bin number, and p_i and λ_i represent the occupancy rate and the firing rate of the ith bin, respectively. Finally, λ denotes the mean firing rate. The probability of obtaining the spatial information score was calculated from the random distribution of spatial information using a Monte-Carlo method. That is, the spiking train of a unit was randomly shifted (minimum shifting unit = 33 s), and spatial information was re-calculated from the generated rate-map for each shift. This procedure was repeated for 1000 times. The p-value was defined as the proportion of shuffled data above the spatial information obtained from the actual rate map. The coherence was measured as the correlation coefficient between raw rate map and reconstructed rate map, where the firing rate of each pixel was averaged firing rate of adjacent pixels. The firing rate (sleep) was measured during sleep session after behavioral experiment. For statistical comparison (ANOVA, repeated-measures ANOVA, t-test, paired t-test and one-sample t-test), commercial software packages including the JMP (SAS), Statview (SAS) and Matlab (MathWorks) were used.

Apparatus for lesion study

An elevated t-maze (72 × 8 cm for stem and 40 × 8 cm for each arm) was used[3]. A food well (2.5 cm diameter, 0.8 cm deep) was located at the end of each arm. The food well was covered by a plastic washer to prevent the rat from sampling a reward in the food well from the stem. A quarter piece of cereal (Froot Loops, Kellogg's) was used as a reward. The arms of the maze were surrounded by an array of 3 LCD monitors. At the end of the stem, a start box with a guillotine door was placed. Infrared sensors were installed in front of the start box and in the stem to measure latency. The behavioral experiment was controlled by Matlab-based custom program and the sensor data were acquired using a data acquisition device (PCI-6221, National Instrument, Austin, Texas). Five visual scenes were used in the behavioral experiments: black screen, zebra, pebbles, peacock, and palm-tree patterns. During pre-training and OLD sessions, zebra and pebble scenes were presented, and the rewarding arm was fixed to one of the arms associated with the scene (i.e., left arm for zebra scene and right arm for pebbles scene). In the NEW session, peacock and palm-tree scenes presented across trials (peacock for the left arm and palm trees for right arm). The scene pairs (zebra-pebble and peacock-palm trees) and their associated reward locations (left and right arms) were pseudo-randomly assigned to the rats. The maze was located within a circular curtained area in which white noise was played through loudspeakers. After each session, the maze was vacuumed and swiped with 70% ethanol.

Behavioral paradigm

Handling and shaping After 5 days of handling and foraging in a laboratory cart, a rat experienced a habituation session in the maze. During habituation, the rat freely explored the maze and collected cereal rewards scattered throughout the maze to get familiarized to the maze and environment. Once acquainted, a shaping session started in which the rat learned to run directly to a food-well to find the reward underneath the washer covering the food-well once the start box was opened by an experimenter. Access to one of the arms was blocked by a transparent acrylic block within a session and the other arm was blocked in the next session, and so forth. When rat ran 90 trials in total in the habituation session, pre-training started.

Pre-surgical training with old scenes A training session was composed of sample and test blocks. There were five sample blocks (10 trials for each block). Two scenes (zebra-pebbles or peacock-palm trees) were alternately presented across the sample blocks except between the first and second blocks (i.e., black screen for the first block). Rewarding arms were identical between the first and second sample blocks. During the sample blocks, access to the unrewarded arm was blocked by a transparent acrylic block. After the last sample block, the testing block commenced (40 trials) without delay. In the testing block, both arms were accessible from the stem and one of the two scenes from the sampling block appeared pseudo-randomly across trials. When the rat reached criterion (accuracy for both scenes > 75%), the animal was assigned to either the lesion group or the control group for surgery.

Neurotoxic lesion Colchicine was injected into the FC for the lesion group[8,9] (n = 8), whereas sterilized saline was injected in the control group (n = 8). For surgery, the rat was first anesthetized by sodium pentobarbital (Nembutal, 65 mg/kg, I.P.) and its head was fixed in a stereotaxic instrument (Kopf Instruments, Tujunga, CA). Anesthesia was maintained by 1-2% isoflurane (Piramal, Bethlehem, PA). Small burr holes were drilled to inject colchicine (7 mg/mL) or sterilized saline (0.05 μL per injection site at 10 μl/h rate; microinjection pump KDS-101, KD Scientific) through a glass pipette (HSU-2920109, Marienfield) connected to a 10 μl Hamilton syringe via polyethylene tubing (PE20, Becton Dickinson). The following coordinates were used for drug injection: 3.4 mm posterior to bregma, ±1.2 mm lateral to the midline, and 4.2 mm ventral from dura at ± 20° angle. It is well known that colchicine is a neurotoxin that selectively ablates granule cells in the dentate gyrus. Some studies reported damage outside the DG (e.g., CA1) by colchicine[10,11], but we did not find any volume shrinkage in other areas in the hippocampus. After surgery, the rat rested for 3 days, and handling and cart foraging procedures began again. Ten days after surgery, the habituation session (90 trials) was carried out for 4 days to help the rat to re-adapt to the experimental situation.

Post-surgical test (main task) Post-surgical test started 14 days after surgery and the testing procedures were identical with those in the pre-surgical training except that no correction was allowed. On D14 (OLD1) and D18 (OLD2), old scenes (zebra-pebble or

peacock-palm trees) were presented to test retrieval of memory. On D16 (NEW), a new pair of scenes that had not been presented during the training period was used to test memory acquisition.

Histological analysis Histological procedures were the same with the ones described for the electrophysiological experiments except that only every third sections were collected during sectioning. To quantitatively assess the amount of lesion using volumetry, principal cell layers in the CA1, CA2/3, DG in the hippocampus were traced using the photomicrographs (1x magnification) using Photoshop (Adobe). The subregion-specific area was measured by ImageJ software (NIH). The total hippocampal volume was estimated by considering the depth (40 μm) of the histological section and the sampling frequency (every third). The tissue range for volumetry was approximately from 2.9 mm to 4.7 mm posterior to bregma. For the FC volumetry, photomicrographs taken with 10x magnification were used. The procedures for volume measurement for the FC were different from those for the other subregions. This was largely because of the low density of cells with small cell bodies in the FC. That is, tracking the boundaries of the cell layers in the FC in the same way for other cell layers of the hippocampus did not reflect the actual volume of the FC accurately. Therefore, we converted the colored photomicrograph to black-and-white photo and set a threshold at which only the contours of neurons were visible. Measuring the dark areas in the photo afterward yielded good volumetric estimate of the FC (Supplementary Figure 2). One of the rats in the lesion group was excluded from analysis for the lack of lesion. Two rats whose lesions were extensive were also excluded. As a result, five rats were assigned to the lesion group with eights rats assigned to the control group (Supplementary Table 4).

Analysis of behavioral data To compare behavioral performance between the control and lesion groups, a repeated-measures mixed ANOVA and t-test (both paired and unpaired) were conducted using Statview software. Latency was measured from the opening of the start-box door to displacing the washer over the food-well or to the last sensor on the track. One rat in the control group was excluded from the latency analysis due to its relative latency was too deviated from the mean of the control group more than 2 SD. But the trend was maintained even in this rat (trial 10 latency: 0.96s, trial 11 latency: 7.17s) To confirm the

categorization of the lesioned rats into the normal and extensive lesion groups, we conducted a K-Mean clustering with JMP 11 (SAS; Parameter: FC volume, NEW performance, latency). For presenting the data and statistical results, mean and standard errors (mean ± S.T.E) were used.

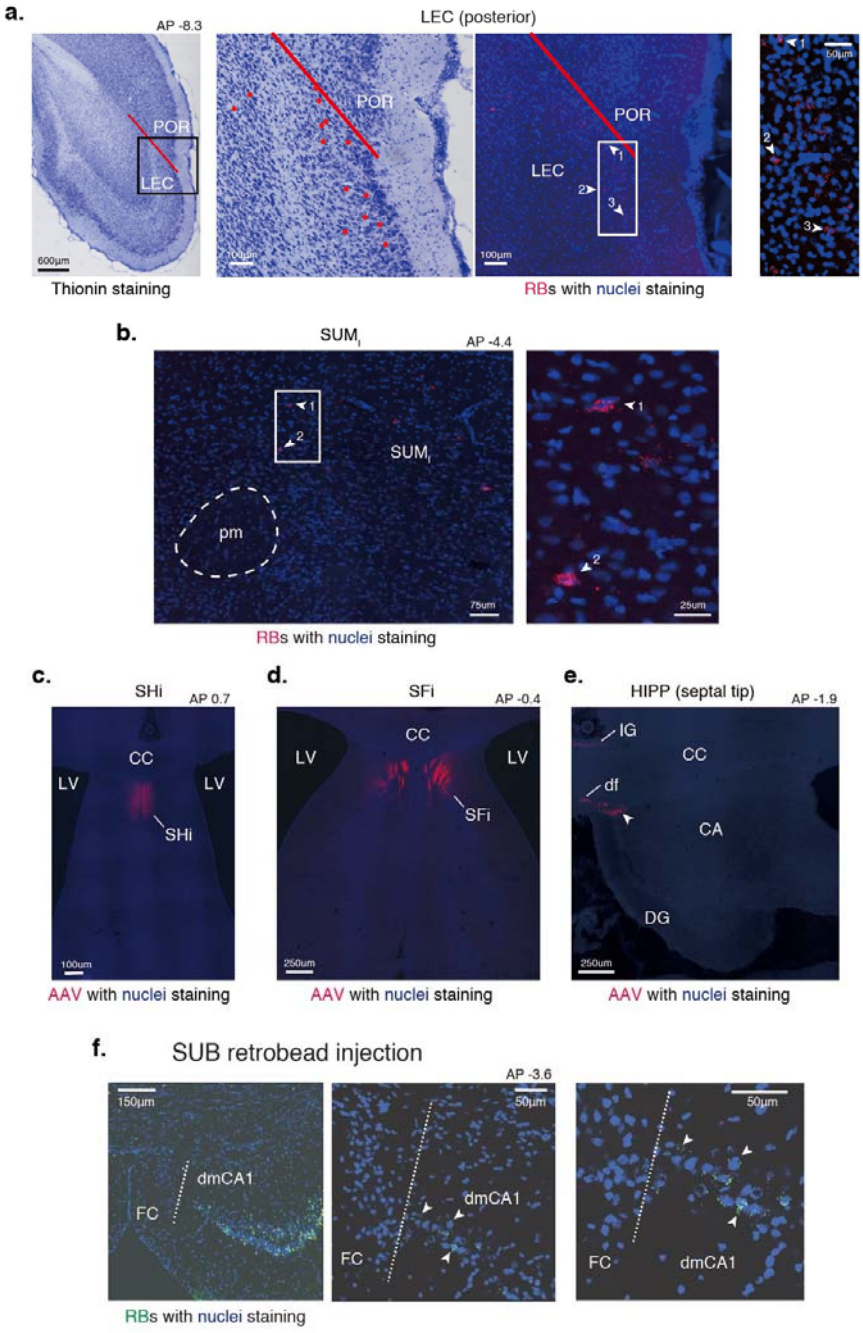

Supplementary Figure 1. Afferent and efferent connection of the FC. a. Afferent projection of the FC from the posterior LEC. The first picture shows the overall cortical structure and the boundaries between the LEC and POR (red line). The second one is the enlarged picture of the box located in the first picture followed by an adjacent fluorescent

stained section. Red dots denote the location of retrobead-positive cells shown on the fluorescent section. The last picture is an enlarged view of the white box in the third picture. **b.** Retrobeads injected into the FC were detected in the lateral part of the supramammillary body. The projection is supported by SUM anterograde tracing study[12] **c-e**. Efferent connections of the FC to the SHi, SFi, IG, df, and septal tip of the hippocampus (white arrow head). The septal tip region is also named SFi in an atlas[13]. **f.** *(left)* Afferent subiculum projection from the distalmostCA1 are shown. The green retrobeads were located in the CA1 but not in the FC, showing the distinct anatomical borders between the CA1 and FC. *(center and right)* A magnified view of the borer between the FC and dmCA1. Abbreviations: POR = postrhinal cortex, LEC = lateral entorhinal cortex, SUM_l = supramammillary nucleus (lateral parts), pm = principal mammillary tract, SHi =septohippocampal nucleus, SFi = septofimbrial nucleus, LV = lateral ventricle, CC = corpus callosum, IG = indusium griseum, df = dorsal fornix ,CA = cornus ammonis, DG = dentate gyrus, SUB = subiculum, dmCA1 = distalmostCA1

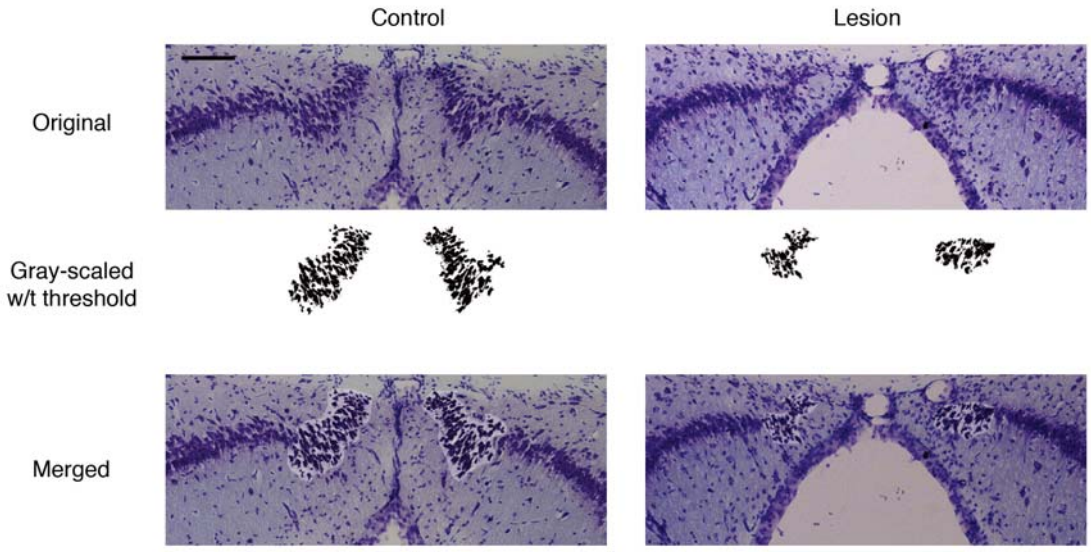

Supplementary Figure 2. Volumetric measurement of the FC. Original photomicrographs taken with 10x magnification are shown in the first row (Original). Clusters of FC cells isolated from the background by setting an intensity threshold in the black-and-white photos of the original photomicrographs. The bottom row shows the merged photo of the two above to verify the locations of the FC in the original photos. Scale bar = 100 μm

Supplementary Table 1. Primary antibodies used in the current study

Antibodies	Host	Working dilution	Company	Catalog number
RGS14	Mouse IgG2a	1:300	NeuroMab	#75-170 (RRID: AB_2179931)
WFS1	Rabbit	1:300	proteintech	11558-1-AP
NeuN	Mouse IgG1	1:500	millipore	cat.MAB377
NG2	Rabbit	1:500	millipore	cat.AB5320
BrdU	Mouse	1:300	Thermo Fisher Scientific	MA3-071
BrdU	Rat	1:500	Abcam	Ab6326

Supplementary Table 2. Statistical result of electrophysiological experiment. Asterisks in the p-value column indicate statistical significance. Bonferroni correction was conducted (corrected alpha = 0.166). Values represent Mean ± S.E.M. AVG = average.

Measurement	FC	dmCA1	dCA1	Test	Statistics	df	p-value	FC/dmCA1	FC/dCA1	dmCA1/dCA1
Spike width (μs)	321.1±6.5	383.1±3.5	397.0±5.9	ANOVA, Bonferonni	37.5	2, 331	P<0.0001*	P<0.0001*	P<0.0001*	P=0.0284
Firing rate (sleep, Hz)	0.478±0.075	0.596±0.045	0.704±0.073	ANOVA, Bonferonni	2.135	2, 331	P=0.1199	P=0.2598	P=0.0460	P=0.1770
AVG. firing rate (square field, Hz)	0.518±0.057	0.884±0.066	0.893±0.087	ANOVA, Bonferonni	4.032	2, 331	P=0.0186*	P=0.0072*	P=0.0105*	P=0.9345
Peak firing rate (Hz)	3.937±0.400	6.391±0.354	6.509±0.481	ANOVA, Bonferonni	6.102	2, 331	P=0.0025*	P=0.0011*	P=0.0015*	P=0.8336
Spatial information (Bits/Spike)	0.992±0.057	1.195±0.043	1.233±0.061	ANOVA, Bonferonni	3.110	2, 331	P=0.0459*	P=0.0288	P=0.0162*	P=0.5951
Spatial coherence	0.375±0.024	0.490±0.016	0.525±0.025	ANOVA, Bonferonni	7.714	2, 331	P=0.0005*	P=0.0014*	P=0.0001*	P=0.1990
Stability	0.565±0.039	0.648±0.021	0.624±0.031	ANOVA, Bonferonni	1.543	2, 330	P=0.2153	P=0.0816	P=0.2433	P=0.5133
Number of field	1.458±0.940	1.495±0.054	1.385±0.067	ANOVA, Bonferonni	0.797	2, 331	P=0.4514	P=0.7531	P=0.5512	P=0.2077
Field size (cm^2)	654.6±56.1	704.7±32.6	759.8±47.6	ANOVA, Bonferonni	0.981	2, 483	P=0.3758	P=0.4886	P=0.1818	P=0.3227
In-field firing rate (Hz)	1.621±0.150	2.625±0.126	2.778±0.199	ANOVA, Bonferonni	8.018	2, 483	P=0.0004*	P=0.0003*	P=0.0001*	P=0.4743

Supplementary Table 3. Statistical result of the contextual behavior task. Statistically significant results ($p<0.05$) were denoted with asterisk. For statistical comparison, repeated measures mixed ANOVA, t-test and paired t-test were used.

related figure	Mean±S.E.M		N	Statistics	Post-hoc test		note
Fig. 5d (OLD and NEW performance)	OLD1, control	86.3±2.6	8	Surgical condition: F (1, 11) = 5.3, P = 0.042*, Task: F (1, 11) = 35.7, P < 0.001*; Surgical condition X task: F (1, 11) = 9.3, P = 0.011*	Control vs. Lesion in OLD1	t (11) = 0.3, P = 0.760	
	OLD1, lesion	87.8±4.8	5		Control vs. Lesion in NEW	t (11) = 3.5, P = 0.005*	
	NEW1, control	75.8±4.0	8		OLD1 vs. NEW in Control	t (7) = 2.3, P=0.054	
	NEW1, lesion	55.4±3.6	5		OLD1 vs. NEW in Lesion	t (4) = 5.9, P = 0.004*	
				OLD1, control, t (7) = 14.0, P < 0.001*; OLD1, lesion, t (4) = 7.9, P = 0.001*; NEW1, control, t (7) = 6.4, P < 0.001*; NEW1, lesion, t (4) = 1.5, P = 0.205			Comparison with chance (50%)
Fig. 5d (right)	control	10.5±4.5	8	t (11) = 3.1, P = 0.011*			
	lesion	32.4±5.5	5				
Fig. 5e (OLD2 performance)	OLD2, control	91.6±2.7	8	t (11) = 0.1, P = 0.890			
	OLD2, lesion	92.2±2.8	5				
Fig. 5f (NEW, latency)	control	1.93±0.19	8	t (11) = 1.6, P = 0.133			
	lesion	2.40±0.22	5				
Fig. 5h (trial latency, NEW)	control, trial 10	1.19±0.28	7	Surgical condition: F (1, 10) = 0.9, P = 0.377, Trial: F (1, 10) = 6.0, P = 0.034*, Surgical condition X task: F (1, 10) = 9.4, P = 0.012*	trial 10 vs. trial 11, control	t (6) = 3.9, P = 0.008*	
	control, trial 11	2.41±0.59	7		trial 10 vs. trial 11, lesion	t (4) = 0.5, P = 0.661	
	lesion, trial 10	1.38±0.25	5		control vs. lesion, trial 10	t (11) = 0.6, P = 0.577	
	lesion, trial 11	1.24±0.05	5		control vs. lesion, trial 11	t (10) = 1.6, P = 0.131	
Fig. 5i (trial latency ratio, trial 10 based)	trial 11, control	2.01±0.07	7	t (10) = 4.9, P = 0.001*			
	trial 11, lesion	1.06±0.22	5				
	trial 12, control	1.06±0.10	8	t (11) = 0.9, P = 0.383			
	trial 12, lesion	0.92±0.14	5				
				trial 11, control, t(6) = 14.7, P < 0.001* trial 11, lesion, t(4) = 0.3, P = 0.809 trial 12, control, t(7) = 0.7, P = 0.528 trial 12, lesion, t(4) = 0.6, P = 0.575			Comparison with trial 10 (1)

Supplementary Table 4. Statistical description of the FC volumetry. The table below show the number of rats in each group and the volume of the FC (unit: 10^{-3} mm^3). Last two groups were excluded from an analysis due to their lesion status.

Group	N	Mean	S.T.E.
Control	8	26.8	1.9
Lesion	5	11.1	1.8
No lesion	1	28.1	
Extensive lesion	2	6.3	0.2

References for Supplementary Materials

1 Kaspar, B. K. *et al.* Adeno-associated virus effectively mediates conditional gene modification in the brain. *Proceedings of the National Academy of Sciences of the United States of America* **99**, 2320-2325, doi:10.1073/pnas.042678699 (2002).

2 Mattis, J. *et al.* Principles for applying optogenetic tools derived from direct comparative analysis of microbial opsins. *Nature methods* **9**, 159-172, doi:10.1038/nmeth.1808 (2011).

3 Lee, H. W., Lee, S. M. & Lee, I. Neural Firing Patterns Are More Schematic and Less Sensitive to Changes in Background Visual Scenes in the Subiculum than in the Hippocampus. *The Journal of neuroscience : the official journal of the Society for Neuroscience* **38**, 7392-7408, doi:10.1523/JNEUROSCI.0156-18.2018 (2018).

4 Henriksen, E. J. *et al.* Spatial representation along the proximodistal axis of CA1. *Neuron* **68**, 127-137, doi:10.1016/j.neuron.2010.08.042 (2010).

5 Boccara, C. N. *et al.* A three-plane architectonic atlas of the rat hippocampal region. *Hippocampus* **25**, 838-857, doi:10.1002/hipo.22407 (2015).

6 Skaggs, W. E., McNaughton, B. L., Wilson, M. A. & Barnes, C. A. Theta phase precession in hippocampal neuronal populations and the compression of temporal sequences. *Hippocampus* **6**, 149-172, doi:10.1002/(SICI)1098-1063(1996)6:2<149::AID-HIPO6>3.0.CO;2-K (1996).

7 Skaggs, W. E., McNaughton, B. L., Gothard, K. M. & Markus, E. J. in *Advances in neural information processing systems 5*. (eds S.J. Hanson, J.D. Cowan, & C.L. Giles) 1030-1037 (Morgan Kaufmann, 1993).

8 Lee, I. & Kesner, R. P. Differential contributions of dorsal hippocampal subregions to memory acquisition and retrieval in contextual fear-conditioning. *Hippocampus* **14**, 301-310 (2004).

9 Walsh, T. J., Schulz, D. W., Tilson, H. A. & Schmechel, D. E. Colchicine-induced granule cell loss in rat hippocampus: selective behavioral and histological alterations. *Brain Res* **398**, 23-36 (1986).

10 Ahn, J. R. & Lee, I. Intact CA3 in the hippocampus is only sufficient for contextual behavior based on well-learned and unaltered visual background. *Hippocampus* **24**, 1081-1093, doi:10.1002/hipo.22292 (2014).

11 Jarrard, L. E. Use of excitotoxins to lesion the hippocampus: update. *Hippocampus* **12**, 405-414, doi:10.1002/hipo.10054 (2002).

12 Haglund, L., Swanson, L. W. & Kohler, C. The projection of the supramammillary nucleus to the hippocampal formation: an immunohistochemical and anterograde transport study with the lectin PHA-L in the rat. *The Journal of comparative neurology* **229**, 171-185, doi:10.1002/cne.902290204 (1984).

13 Swanson, L. W. Brain maps 4.0-Structure of the rat brain: An open access atlas with global nervous system nomenclature ontology and flatmaps. *The Journal of comparative neurology* **526**, 935-943, doi:10.1002/cne.24381 (2018).